Icarus 290 (2017) 201–214

Contents lists available at ScienceDirect

Icarus

journal homepage: www.elsevier.com/locate/icarus

Deep UV Raman spectroscopy for planetary exploration: The search for in situ organics

William J. Abbey[a], Rohit Bhartia[a,*], Luther W. Beegle[a], Lauren DeFlores[a], Veronica Paez[b], Kripa Sijapati[c], Shakher Sijapati[d], Kenneth Williford[a], Michael Tuite[a], William Hug[c], Ray Reid[c]

[a] Jet Propulsion Laboratory, California Institute of Technology, 4800 Oak Grove Drive Ave, Pasadena, CA 91109, United States
[b] Georgia Institute of Technology, North Ave NW, Atlanta, GA, 30332, United States
[c] Photon Systems Inc.,1512 W Industrial Park St, Covina, CA 91722, United States
[d] University of Wisconsin-Madison, Madison, WI 53706, United States

ARTICLE INFO

Article history:
Received 26 September 2016
Revised 24 January 2017
Accepted 26 January 2017
Available online 1 March 2017

Keywords:
Astrobiology
Mars
Raman spectroscopy

ABSTRACT

Raman spectroscopy has emerged as a powerful, non-contact, non-destructive technique for detection and characterization of in situ organic compounds. Excitation using deep UV wavelengths (< 250 nm), in particular, offers the benefits of spectra obtained in a largely fluorescence-free region while taking advantage of signal enhancing resonance Raman effects for key classes of organic compounds, such as the aromatics. In order to demonstrate the utility of this technique for planetary exploration and astrobiological applications, we interrogated three sets of samples using a custom built Raman instrument equipped with a deep UV (248.6 nm) excitation source. The sample sets included: (1) the Mojave Mars Simulant, a well characterized basaltic sample used as an analog for Martian regolith, in which we detected ~0.04 wt% of condensed carbon; (2) a suite of organic (aromatic hydrocarbons, carboxylic acids, and amino acids) and astrobiologically relevant inorganic (sulfates, carbonates, phosphates, nitrates and perchlorate) standards, many of which have not had deep UV Raman spectra in the solid phase previously reported in the literature; and (3) Mojave Mars Simulant spiked with a representative selection of these standards, at a concentration of 1 wt%, in order to investigate natural 'real world' matrix effects. We were able to resolve all of the standards tested at this concentration. Some compounds, such as the aromatic hydrocarbons, have especially strong signals due to resonance effects even when present in trace amounts. Phenanthrene, one of the aromatic hydrocarbons, was also examined at a concentration of 0.1 wt% and even at this level was found to have a strong signal-to-noise ratio. It should be noted that the instrument utilized in this study was designed to approximate the operation of a 'fieldable' spectrometer in order to test astrobiological applications both here on Earth as well as for current and future planetary missions. It is the foundation of SHERLOC, an arm mounted instrument recently selected by NASA to fly on the next rover mission to Mars in 2020.

1. Introduction

It was recently announced that the Curiosity Rover detected organic compounds in the drill fines collected at Cumberland in Gale Crater, the first definitive detection of organic carbon in surface materials on Mars (Freissinet et al., 2014; Glavin et al., 2015). Yet, despite this amazing success, understanding the source and distribution of organic compounds on the Martian surface has proven to be a technically challenging and frustrating endeavor. In spite of constant meteoritic and interplanetary dust fall throughout Martian history (Flynn, 1996), evidence that photolytic byproducts could survive (Benner et al., 2000; Stalport et al., 2009), and the possibility of abiotic organic matter forming via igneous and/or hydrothermal processes (Steele et al., 2012a; 2012b), to date none of the landed missions to Mars have been able to *directly* detect organic material on the surface. These investigations, including Curiosity's Sample Analysis at Mars (SAM) instrument, all relied on pyrolysis to identify organic material by heating bulk samples of Martian regolith in order to volatilize any organics present for analysis in a gas chromatograph–mass spectrometer (GC–MS) (Biemann and Lavoie, 1979; Boynton et al., 2001; Mahaffy et al., 2012). This technique is complicated by the presence of perchlorate in Martian rocks and soils. Strong oxidizers on the Martian

* Corresponding author.
E-mail addresses: rbhartia@jpl.nasa.gov, rohit.bhartia@jpl.nasa.gov (R. Bhartia).

http://dx.doi.org/10.1016/j.icarus.2017.01.039
0019-1035/

surface, like perchlorate, produce substantial amounts of oxygen when heated, suggesting that pyrolysis in general is not well suited for organic analysis, as the presence of oxygen promotes combustion of organics during heating (Navarro-Gonzales et al., 2010; Ten Kate, 2010; Leshin et al., 2013). When heated, perchlorates alter the structure of the organic compounds so that the identities of the organics remain uncertain (Freissinet et al., 2014; Ming et al., 2014). Also, some key organic compounds are not volatile, such as the carboxylic acids, and would not be directly detectable by GC–MS experiments even without the presence of an oxidizer in the Martian regolith (Benner et al., 2000). Furthermore, destructive bulk analysis techniques, such as pyrolysis, fail to retain the spatial context of in situ samples, an important clue for the interpretation of any organic compounds discovered. Our experience on Mars thus far has demonstrated that alternate methods of exploration are a necessity if future planetary missions intend to detect and study the origin of native organic compounds.

Ultraviolet (UV) and deep UV (< 250 nm) Raman spectroscopy has recently emerged as a potential alternative to destructive bulk processing methods, such as pyrolysis GC–MS, as a powerful, non-contact, non-destructive technique that offers spatially resolved, high sensitivity detection and characterization of in situ organics and associated minerals (Wu et al., 2001; Bozlee et al., 2005; Frosch et al., 2007; Tarcea et al., 2007; Skulinova et al., 2014; Eshelman et al., 2014). Raman spectroscopy is based on the inelastic scattering of incident monochromatic laser light, with the scattering being dependent on the polarizability of the vibrational energy of the molecular bonds within the target, thus enabling their classification (C–C, C–H, C–O, SOx, COx, POx, OH, etc). Visible, infrared, and near-infrared Raman spectroscopy have been proposed as tools for planetary exploration for well over a decade now for the rapid identification of both minerals and potential biomarkers (e.g., Popp et al., 2001; Ellery and Wynn-Williams, 2003; Wang et al., 2003; Jehlicka et al., 2009; Vítek et al., 2009; Alajtal et al., 2010). In fact, visible wavelength Raman spectrometers have been included in the plans for both the European Space Agency's ExoMars Mission (Rull et al., 2011) and SuperCam on NASA's next Mars rover in 2020 (Clegg et al., 2014). In addition, targets can also be excited using wavelengths in the deep UV spectral range, which offers significant signal enhancement over visible and infrared wavelengths, especially for carbonaceous compounds (Asher, 1984; Loppnow et al., 2004), making deep UV Raman spectroscopy particularly well suited for any investigation where detection of organics is of primary interest. A deep UV Raman spectrometer is at the heart of the Scanning Habitable Environments with Raman and Luminescence for Organics and Chemicals (SHERLOC) investigation that has been selected by NASA for inclusion on the arm turret of the Mars 2020 rover to search for organic compounds on the Martian surface (Beegle et al., 2014, 2015).

Deep UV Raman spectroscopy has been a valuable tool for the study of organic compounds for many years, from living bacterial cells to abiotic, aromatic hydrocarbons to amorphous, diamond-like carbon films (e.g., Asher and Johnson, 1984; Nelson et al., 1992; Ferrari and Robertson, 2001). To date, the vast majority of this work has been done with the organics suspended in either a carrier gas, a liquid solution, or as dried samples subject to rotation, with few interrogations performed on static solid samples (Asher et al., 1986; Asher, 1988; Chadha et al., 1993; Wu et al., 2001; Tarcea et al., 2007). The intent of these previous studies was to understand the benefits of deep UV excitation in terms of a fluorescence-free Raman region and the resonance and pre-resonance effects of organic vibrations. As such they used large deep UV laser sources with a fluence (radiant energy received by a surface area) that required continual movement of the sample to avoid thermal decomposition or photolysis of the sample (Asher, 1988; McCreery, 2005; Smith and Dent, 2005). While these laboratory devices are not amenable to field work or *in-situ* investigations, recent technological advances in optics, manufacturing, and laser design have made possible the construction of low energy input, compact, deep UV laser sources and, in turn, compact deep UV Raman instruments (Storrie-Lombardi et al., 2001; Bhartia et al., 2012a; 2012b; Beegle et al., 2014). These instruments can detect organics with decreased fluence on the sample by capitalizing on the resonance effects of organic compounds and the efficiency of Rayleigh scattering at these wavelengths ($1/\lambda^4$), thus minimizing the risk of sample degradation. Loppnow et al. (2004) used deep UV wavelengths (220 nm & 230 nm) to examine aromatic hydrocarbons, both in solution as well as in solid form, with minimal degradation. Kumamoto et al. (2011) also showed that even with a fluence of 400 J/cm^2, sample degradation with UV and deep UV excitation (244 nm) is not detectable, and only achieved spectral degradation of nucleotides and amino acids of dried and hydrated HeLa cells after reaching 4000 J/cm^2. Most recently, Eshelman et al. (2014) and Skulinova et al. (2014) used UV excitation (266 nm & 355 nm, respectively) to detect and identify organic compounds, both in their pure form and mixed within a silica sand matrix, with no apparent degradation using ~1000 J/cm^2, even with a peak power of 49 KW/cm^2.

The purpose of this paper is to demonstrate the utility of deep UV Raman spectroscopy to planetary investigations such as SHERLOC, specifically with regards to the detection and characterization of organic compounds, but also inorganic compounds and minerals that are of astrobiological interest, either as sinks for key organic elements (CHNOPS) or by their likely association with potential biomarkers (i.e., hydrothermal precipitates, evaporite minerals, etc). To assess the fidelity of this technique we examined three types of samples: 1) a mineralogically and organically well characterized basaltic dust used as an analog for Martian regolith; 2) a suite of solid phase organic standards and astrobiologically relevant inorganic standards; and 3) the Martian analog after being spiked with a representative selection of these standards at the 1 wt% and (in one case) 0.1 wt% levels. This third type of sample was used to obtain a preliminary understanding of the technique's sensitivity to these compounds in the face of potential matrix effects that may be found in natural 'real world' environments (i.e., mixed with regolith or sediments). Spectra were obtained for all of the above samples, in either granular, powdered, or pelletized form, with a custom built Raman instrument utilizing an integrated deep UV source (248.6 nm) to excite the target. It is important to note that this instrument was built with optical parameters designed to approximate the performance of a fieldable planetary instrument. The design used in this study, coupled with a compact spectrometer and deep UV native fluorescence, are highly amenable to organic detection implementations relevant to astrobiology field work, as well as current and future planetary missions such as Mars 2020.

2. Materials

2.1. The Mojave Mars simulant

The Martian analog used in this study was the Mojave Mars Simulant (MMS). This basaltic simulant was developed at JPL to stand in for Martian regolith and has been shown to be similar in both chemical and mineralogical character to basalts found on Mars (Peters et al., 2008). More specifically, for this study, we chose to use the MMS Dust, the fine-grained size fraction of MMS collected after the bulk rock has been pulverized. In brief, the MMS is an olivine basalt mined from the Tertiary Tropico Group near Boron, California in the western Mojave Desert (Dibblee, 1958, 1967). It is dominated by plagioclase feldspar (~37 wt%), Ca-rich pyroxene (~17 wt%), basaltic glass (~41 wt%), minor amounts of magnetite (≤5 wt%), and trace amounts (<2 wt%) of Fe-rich olivine,

Table 1
Organic and inorganic compounds examined in this study using deep UV Raman spectroscopy.

	Class	Compound/Mineral/Species	Formula	Source
Organic compounds	Aromatic Hydrocarbons	Biphenyl	$(C_6H_5)_2$	Aldrich #B34656, purity 99.5% (*Lot 11524CB*)
		Naphthalene	$C_{10}H_8$	Sigma-Aldrich #147141, purity 99% (*Lot 06004TH*)
		Anthracene*	$C_{14}H_{10}$	Sigma-Aldrich # 141062, purity 99% (*Lot 06619JE*)
		Phenanthrene*	$C_{14}H_{10}$	Sigma #P2528, purity > 96% (*Lot 052K1449*)
		Pyrene	$C_{16}H_{10}$	Sigma Life Science #82648, purity ≥ 99% (*Lot BCBF4410B*)
		Perylene	$C_{20}H_{12}$	Aldrich #P11204, purity ≥ 99% (*Lot 04101PGV*)
	Carboxylic Acids	Palmitic Acid*	$CH_3(CH_2)_{14}COOH$	Supelco #R420160, purity 99.6% (*Lot LB40764*)
		Phthalic Acid	$C_6H_4(COOH)_2$	Sigma-Aldrich #402915, purity ≥ 99.5% (*Lot BCBK8052V*)
		Mellitic Acid	$C_6(COOH)_6$	Aldrich #M2705, purity 99% (*Lot 08205PO*)
	Amino Acids	Glycine*	$CH_2(NH_2)COOH$	Sigma-Aldrich #33226, purity 99.7–101% (*Lot 70650*)
		Serine	$CH_2CH(NH_2)COOH(OH)$	Sigma Life Science # 84959, purity ≥ 99.5% (*Lot 1349921 V*)
		Histidine*	$CH_2CH(NH_2)COOH(C_3H_3N_2)$	Sigma #53319, purity 99.5% (*Lot 13CBF7717V*)
		Tyrosine	$CH_2CH(NH_2)COOH(C_6H_4OH)$	Sigma Life Science #T8566, purity 99.0% (*Lot 109K0032*)
		Tryptophan	$CH_2CH(NH_2)COOH(C_8H_6N)$	Sigma #T-0254, purity 98% (*Lot 102K0370*)
Inorganic Compounds	Sulfate Minerals	Gypsum*	$CaSO_4{\cdot}2H_2O$	Tawas City, Michigan (WARDS *#46–3798*)
		Mg-hydrated sulfates[a]	$MgSO_4{\cdot}nH_2O$	Sigma Aldrich #434183, purity ≥ 97% (*Lot unknown*)
		Fe-hydrated sulfates[b]	$FeSO_4{\cdot}nH_2O$	Malinckrodt #5056, purity ≥ 98% (*Lot 5056 T41581*)
	Carbonate Minerals	Calcite	$CaCO_3$	Santa Eulalia, Chihuahua, Mexico (WARDS *#49–5860*)
		Magnesite*	$MgCO_3$	Brumado, Bahia, Brazil (WARDS *#49–5923*)
		Ankerite-Dolomite	$Ca(Fe, Mg)(CO_3)_2$	Charlemont, Massachusetts (Excalibur Mineral Corp)
	Phosphate Minerals	Fluorapatite*	$Ca_5(PO_4)_3F$	Durango, Mexico (WARDS *#49–5855*)
		Chlorapatite[c]	$Ca_5(PO_4)_3Cl$	Odegarden Verk, Bamble, Norway (JPL collection)
	Nitrates	NH_4-nitrate	NH_4NO_3	Fisher #A676500, purity ≥ 98% (*Lot 984670*)
		Na-nitrate	$NaNO_3$	J.T. Baker #1–3770, purity ≥ 99.0% (*Lot 508663*)
		K-nitrate*	KNO_3	Malinckrodt #7028, purity ≥ 99.0% (*Lot 7028 T22620*)
	Perchlorates	K-perchlorate*	$KClO_4$	Aldrich #24,183–0, purity ≥ 99% (*Lot DA11625BA*)

* compounds used to spike MMS Dust samples at the ~1 wt% level (note: phenanthrene also examined at the ~0.1 wt% level)
[a] kieserite ($1H_2O$) with trace amounts of pentahydrite ($5H_2O$) and hexahydrite ($6H_2O$)
[b] melanterite ($7H_2O$) with subordinate rozenite ($4H_2O$) and trace amounts of szomolnokite ($1H_2O$)
[c] contains < 10 wt% fluorapatite

ilmenite and hematite. Electron microscopy also suggests the presence of very minute concentrations (<1 wt%) of sulfate, carbonate and phosphate. Zeolites have also been reported in the literature (Wise and Kleck, 1988). The MMS Dust is characterized by angular particles, almost conchoidal in fracture habit, generally less than 150 μm in grain size, with the bulk of the particles (>60 wt%) averaging less than 50 μm in size. For this study, additional X-ray diffraction analyses were performed on the MMS Dust to augment the information available in Peters et al. (2008); specifically, mineral phases and glass content (above, in wt%) were more rigorously quantified. The total concentration of carbon-bearing compounds in the MMS was determined by pyrolysis-EGA to be approximately 0.34 wt%, with ~0.04 wt% (400 ppm) originating from the total organic carbon content and ~0.30 wt% originating from carbonate.

2.2. Organic standards

Organic standards chosen for this study include polyaromatic hydrocarbons (PAHs), carboxylic acids and amino acids (see Table 1). All of these organic compounds are expected to be present on the Martian surface due to meteoritic and interplanetary dust fall even in the absence of biotic synthesis (Benner et al., 2000; Botta and Bada, 2002), if not on the surface, where various photochemical processes may destroy them (Stoker and Bullock, 1997), than possibly at depth. Many of these organic compounds have even been identified in Martian meteorites (e.g., Glavin et al., 1999; Steele et al., 2012a); most famously in Allan Hills 84001, where aromatic hydrocarbons, such as anthracene, phenanthrene, pyrene and perylene, were reported in association with putative microfossils (McKay et al., 1996; Becker et al., 1999). Benner et al., (2000) also suggested that oxidation processes on the surface of Mars would convert any aromatic hydrocarbons present, as well as any kerogen, into various derivatives of carboxylic acid, most notably mellitic acid (benzene-1,2,3,4,5,6-hexacarboxylic acid) and phthalic acid (benzene-1,2-dicarboxylic acid), with as much as several kilograms having been potentially generated per square meter of Martian surface over the past 3 billion years, making these key compounds of interest for future astrobiological investigations on Mars. While the long term survivability of amino acids on the Martian surface and near subsurface (to ~ 1 m) is up for debate (Pierazzo and Chyba, 1999; Kminek and Bada, 2006; ten Kate et al., 2006), they are biologically important organic compounds that are vital to basic energy production and transfer cycles, as well as biosynthesis, and are considered essential 'building blocks' for life (Jenkins et al., 2005). All organic standards used in this study are listed in Table 1 and were obtained from the noted chemical supply companies.

2.3. Inorganic standards

Inorganic standards chosen for this study include sulfate minerals, carbonate minerals, phosphate minerals, nitrates and perchlorates (see Table 1). Sulfate minerals, such as gypsum and polyhydrated magnesium sulfates, are believed to be ubiquitous on Mars and may represent ancient acidic lake evaporite deposits (Swayze et al., 2008; Wray et al., 2011; Ehlmann and Edwards, 2014). Most recently, veins of a calcium sulfate (e.g., gypsum) have been found by Curiosity in sedimentary rocks at Gale Crater (Vaniman et al., 2013; Ehlmann and Edwards, 2014). Calcium, magnesium and iron carbonates, while not as wide-spread as sulfates, have been found in the Isidis Basin, the Columbia Hills, and in impact craters across the southern highlands (Ehlmann et al., 2008; Niles et al., 2013). Mg-carbonate also has been reported in Martian dust (Bandfield et al., 2003) and Ca-carbonate has been reported in soils at the Phoenix landing site (Boynton et al., 2009). Phosphate minerals have been identified both on the Martian surface and in Martian meteorites, with chlorapatite believed to be the dominant phase for both (Adcock et al., 2013). Nitrates have yet

to be definitively identified on Mars; however, recent SAM results from Curiosity have suggested their presence (Navarro-Gonzalez et al. 2013; Stern et al., 2015). If true, this would add evidence to the steady-state model of nitrogen in the atmosphere proposed by Manning et al. (2008), with significant implications for the habitability of the planet. Perchlorates were first confirmed at the Phoenix landing site (Hecht et al., 2009), and are suspected to have interfered with organic detection experiments on past rovers and landers (Navarro-Gonzales et al., 2010; ten Kate, 2010; Leshin et al., 2013). All inorganic standards used in this study are listed in Table 1. Salts such as nitrates and perchlorates were obtained from the noted chemical supply companies, while most minerals, except where indicated, are natural samples obtained from the listed mineral suppliers. All mineral phases were verified by X-ray diffraction, and poly-mineralic samples are noted.

2.4. Spiked samples (MMS+Standards)

Samples of MMS Dust were each mixed with approximately 1 wt% or 0.1 wt% of an individual standard for further investigation. Standards were chosen to represent each of the 'classes' defined in Table 1. Particle sizes for both organic and inorganic standards averaged less than 100 µm, on par with the particle size of the MMS Dust (dust particles generally being $< 150\,\mu$m). Spiked samples (~500 mg each) were then pressed into 13 mm diameter pellets, under 8 t of pressure, for approximately one minute, using a Carver model 3752 manual hydraulic press with a SPEX SamplePrep model 3613 die set. Pelletizing was done to reduce the concentration of void spaces in the sample, providing a greater and more uniform cross-sectional area for interrogation. It also served to maintain the well-mixed nature of the samples during analysis. This well-mixed nature was verified by comparing phenanthrene-spiked pellets with un-spiked pellets under ultraviolet illumination. Phenanthrene particles were observed to be evenly distributed throughout the pellets. Finally, in order to make sure that pellitizing had not altered the standards or the MMS Dust in any significant way, pellets were made from pure standards and un-spiked dust, and their Raman spectra compared to that of their un-pelletized counterparts. No significant differences were noted. In addition, un-spiked MMS Dust samples were examined by X-ray diffraction both before and after pellitizing and, likewise, no significant differences were noted.

3. Methods

3.1. X-Ray diffraction (XRD)

Powder X-ray diffraction patterns were obtained for both the mineral standards and the MMS Dust using a Bruker AXS model D8 Discover X-ray diffractometer equipped with a graphite monochromator and a General Area Detector Diffraction System. Radiation applied was CuKα ($\lambda = 1.5404$ Å) operated at 40 kV and 20 mA. Phase identification was accomplished by comparing the 13–75° 2θ range with standard powder diffraction files from the International Centre for Diffraction Data (2000) using the DIFFRAC^{plus} EVA 13 Evaluation Package from Bruker AXS (2007). The relative abundance for each phase present in the mineral standards was determined using the reference intensity ratio (RIR) method (Chung, 1974), using RIR values available in the literature. No attempt was made to quantify mixed hydrates of the same compound (i.e., polyhydrated Mg- or Fe-sulfates) beyond a qualitative assessment. For the MMS Dust, quantitative mineralogy, including the abundance of X-ray amorphous glass, was determined by Rietveld refinement (Rietveld, 1969; Hill and Howard, 1987), using Topas 4 Structure Analysis Software (Bruker AXS, 2008) and the fundamental parameters approach (Cheary and Coelho, 1992).

3.2. Inorganic & organic carbon analysis

Total organic carbon (TOC) for carbonate-free MMS Dust was determined using a Costech 4010 elemental analyzer coupled to a Thermo Fisher Delta V Plus stable isotope ratio mass spectrometer via a Conflo IV interface. To remove carbonate from the sample, the dust was first acidified in excess 1 N HCl and then heated to 50 °C for 24 h. The sample was then centrifuged and the supernatant decanted. Deionized water was added and the sample was vortexed and centrifuged again. This cycle was repeated three times after which the sample pH was neutral. The sample was then dried at 50 °C for 24 h. Subsequently, the carbonate-free residue was weighed into tin capsules and converted to CO_2 for analysis. Acetanelide was used as the standard for C mass determination. The mean range of values between duplicate samples for TOC was less than 2% of the measured abundance. Carbonate contribution was estimated by comparing mass of the dust both before and after acidification.

3.3. Deep UV Raman spectroscopy

Spectra for all samples were collected using MOBIUS, a custom built, deep UV-resonance Raman instrument (Fig. 1). The samples were illuminated with a 248.6 nm NeCu laser (Photon Systems Inc.), injected into the optical path with an edge filter (Semrock Inc), and focused with a deep UV chromatically corrected objective lens (ThorLabs LMU-5x-UVB) with a numerical aperture (NA) of 0.13. Deep UV Raman scattered light was collected at a 180° backscatter geometry and injected into a 550 mm focal length spectrometer using a 0.08 NA objective lens (ThorLabs LMU-3x-UVB) through a 250 µm slit. Since the intent of the instrument was to approximate the performance of a fieldable planetary instrument, an 1800 lines/mm grating coupled to a e2v 42–10 CCD was used to generate a spectrum with a resolution of ~50 cm^{-1}. The e2v detector was liquid nitrogen cooled to approximately −130 °C.

The organic and inorganic standards in Table 1 purchased from chemical supply companies were interrogated in their commercially available granular or powdered forms; while the generally coarser natural mineral standards were powdered by hand in an agate mortar and pestle prior to examination. Spectra of these samples were collected with an accumulation time of 30 sec (except for histidine; see Fig. 3), a laser pulse rate of 40 Hz, over a spot size diameter of $\sim 80\,\mu$m, with a total energy of 3 mJ or a fluence at the sample of 59 J/cm^2. Multiple spectra were taken for each sample so that pulses could be averaged during data processing; the total number of spectra taken for an individual sample was dependent on its signal strength (2 spectra for strong signals, up to 5 spectra for weaker signals). While the pellets of MMS, both spiked and un-spiked, were well-mixed, the concentration within a beam diameter may not have been representative of the actual concentration and thus the pellets were interrogated by taking a 'moving average' over a 0.3 cm^2 area (20% of the full pellet area). Specifically, the pellet was kept in continuous motion under the excitation beam while spectra were acquired at a pulse rate of 20 Hz for a total deposited energy of 9 mJ. It should be noted that this was not done to mitigate sample degradation due to high fluence on the sample, but rather to simulate a large array random point map in the absence of an automated sample stage.

Validation of the wavenumber axis was obtained by calibrating the spectrometer to both the secondary laser line at 252.93 nm (683 cm^{-1} for 248.6 nm excitation) (McNeil et al., 1978) and the atmospheric nitrogen peak at 2330 cm^{-1} (Burris et al., 1992). All spectra are presented as smoothed spectra using a simple unweighted 10 point smoothing function. It should be noted that no background subtractions were performed on any spectra in this study in order to help demonstrate the inherently low background

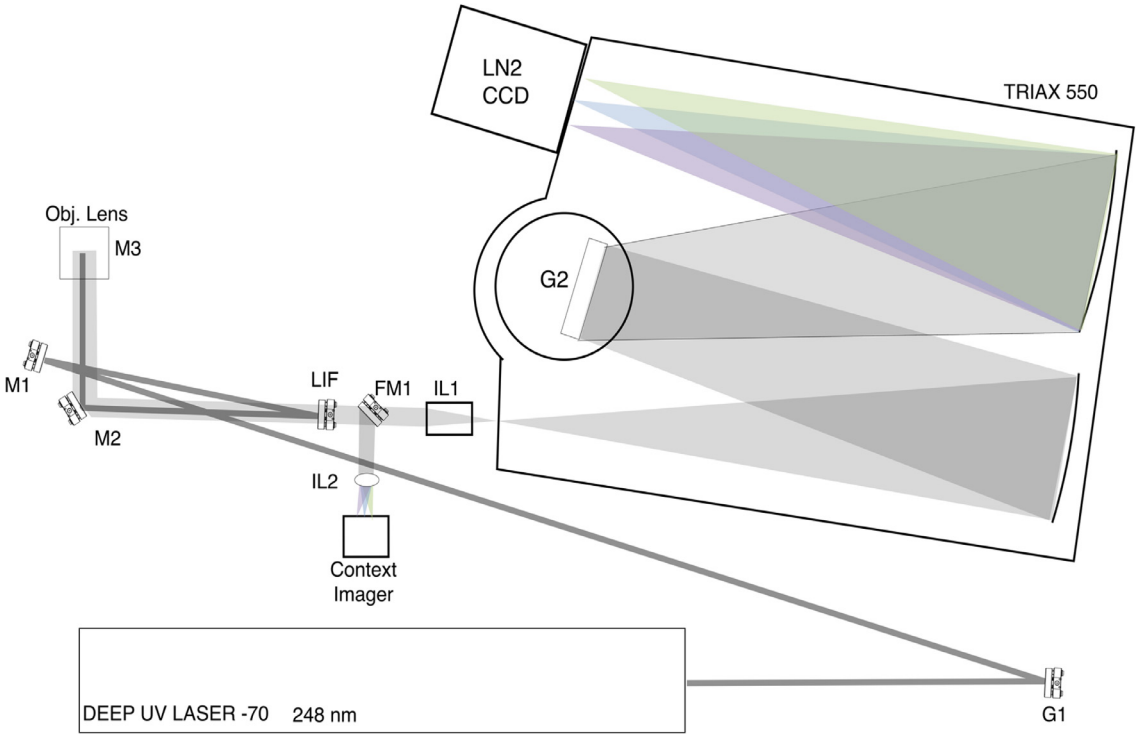

Fig. 1. Block diagram of the MOBIUS deep UV Raman instrument assembled at the Jet Propulsion Laboratory. Used for the collection of all spectra in this study. The deep UV source is a 248.6 nm NeCu laser, G1: 1200 g/mm grating, M1: mirror, LIF: laser injection filter, M2 & M3: broadband reflective mirrors, Obj. Lens: Thor Labs 5x deep UV objective lens, FM1: flip mirror for visible context imaging, IL1 Thorlabs 3x deep UV objective lens, IL2: imaging lens for context imager, Triax 550: 550 mm focal length spectrometer with G2 at 1800 g/mm and a LN2-cooled e2v 42–10 back-thinned back-illuminated UV CCD (UV quantum efficiency 50–60%), Context Imager: Edmund Optics 5 K CMOS color imager. (Note: system also capable of collecting UV fluorescence data).

fluorescence, discussed in more detail below, that is characteristic of the deep UV spectral region. While Raman data were collected for the spectral interval 250 to 3950 cm^{-1}, for the sake of comparison, spectra are only shown in the ~750 to 1750 cm^{-1} range, the so called "fingerprint region" (Jenkins et al., 2005; Zhu et al., 2011), as our long term interest is not only in being able to detect these compounds, but also in differentiating and characterizing them as well. Peak position sensitivity for this spectrometer has been determined to be approximately 4 cm^{-1}, or 1/10 the 50 cm^{-1} spectral resolution of the system's CCD detector (Carter and Pemberton, 1995).

4. Results & discussion

4.1. Analysis of the Mojave Mars simulant (Basaltic dust)

In order to fully explore the use of deep UV Raman spectroscopy for in situ planetary investigations, we first examined the Mojave Mars Simulant (MMS), a basaltic dust that has been used in the past as an analog for Martian regolith (e.g., Anderson et al., 2009; Beegle et al., 2010; Ladino and Abbatt, 2013). The MMS spectra (Fig. 2) reveal peaks consistent with the presence of several carbon-bearing compounds. This carbon is native to the sample (not added) and represents environmental contributions such as atmospheric influx, local diesel exhaust, biotic input, etc. Peaks include a broad carbon-carbon (C–C) vibrational mode centered around 1060 cm^{-1} and the so-called "G-band" or graphitic carbon peak which appears between 1608 and 1640 cm^{-1} (Chu and Li, 2006), as well as a potential carbonate band rising above the C–C stretch at ~1091 cm^{-1} (Rividi et al., 2010). Atmospheric oxygen can also be seen in the MMS spectra at a peak position of about 1554 cm^{-1} (Asher, 1988). The organic carbon bands assigned in these spectra (C–C & G-band) demonstrate several interesting features unique to UV Raman spectroscopy when it is applied to certain organic compounds. The first is the appearance of a broad C–C stretch centered at 1060–1100 cm^{-1} (Gilkes et al., 1997; Ferrari and Robertson, 2000) and the second is the shift of the G-band, typically present at about 1580 cm^{-1} under visible excitation, to as high as 1690 cm^{-1} under deep UV excitation (Merkulov et al., 1997; Ferrari and Robertson, 2001). Both of these features only manifest under UV irradiation and can be attributed to the vibration of tetrahedrally coordinated, amorphous carbon (Gilkes et al., 1997; Merkulov et al., 1997; Chu and Li, 2006). In addition, some spectra show bands at ~952 cm^{-1}, most likely due to the out-of-plane deformational vibrations of carbon-hydrogen (CH) groups (Socrates, 2001). Total concentration of carbon-bearing compounds in the MMS Dust was determined to be approximately 0.34 wt%, with ~0.30 wt% representing carbonate and ~0.04 wt% (400 ppm) detected in the TOC measurement.

Such low concentrations of material can be resolved because deep UV Raman scattering occurs in a spectral region with little or no background fluorescence (Asher and Johnson, 1984; Tarcea et al., 2007). Native fluorescence stimulated by excitation wavelengths of less than ~270 nm, leads to a fluorescence free Raman region (Asher, 1993; Bhartia et al., 2008). Fluorescence emissions resulting from organics extend down to 275 nm while emissions from inorganics and minerals, typically occurs at longer wavelengths > 360 nm (Frosch et al., 2007; Bhartia et al., 2010). This provides for nearly complete separation of the Raman and fluorescence emission bands, allowing for lower background noise and, thus, higher signal-to-noise ratios. Furthermore, the Raman cross-section of a given compound is proportional to the inverse fourth power of the excitation wavelength ($1/\lambda^4$; Rayleigh Law), resulting in an increase in Raman intensity when using the shorter UV wavelengths (Albrecht and Hutley, 1971). To compare, Raman scattering efficiency for the deep UV spectral region (at 248 nm) is

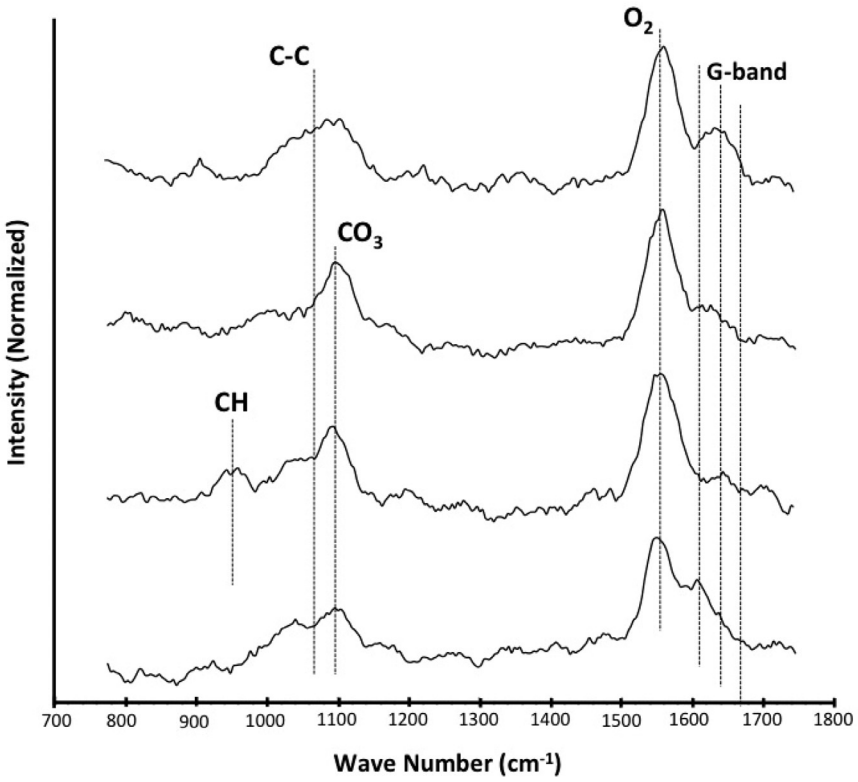

Fig. 2. Deep UV Raman spectra (248.6 nm) of the Mojave Mars Simulant (MMS) Dust, in pellet form, showing bands associated with native organic compounds (C–C, G-band) and trace carbonate (CO_3), as well as atmospheric oxygen (O_2). Spectra were collected on four different pellets using a 300 sec 'moving average' (see Methods) and a 20 Hz pulse rate. Individual spectra normalized to strongest peak and stacked for comparison.

approximately one order of magnitude greater than that for the visible region (at 532 nm), and two orders of magnitude greater than for the near infrared spectral region (at 785 nm). In addition, vibrational modes may be enhanced if their transition energies match that of the incident excitation laser, dramatically improving the scattering cross-section of the interrogated material, and increasing signal strength by as much as seven orders of magnitude (Asher, 1988; Nelson and Sperry, 1991). Many organic and inorganic compounds of interest to planetary exploration have strong absorption bands in the deep UV (e.g., PAHs, amino acids, nitrates, etc) and commonly exhibit these resonance enhancement effects when excited at UV wavelengths (Frosch et al., 2007; Tarcea et al., 2007; Bhartia et al., 2008). Combining these enhancement factors, even while lowering incident energies to avoid sample damage, the signal strength for deep UV Raman spectroscopy can be as much as 10 to 100 times greater than that achieved with more conventional (i.e., visible and infrared) Raman spectroscopy.

4.2. Analysis of organic and inorganic standards

Raman spectral features can be as narrow as a few wavenumbers. As such, the spectral resolution used here enables both detection and classification of the dominant features associated with aromatics, carboxylic acids, amino acids and minerals. These features represent structural information and it is our intention to identify prominent spectral bands revealed under deep UV excitation that may act as 'fingerprints' for the classes of compounds examined in this study. These results are graphically summarized in Fig. 3. Of the aromatic compounds examined, most are dominated by a benzene ring stretching mode that occurs between 1600 and 1685 cm^{-1}. This includes two of the carboxylic acids, as well as aromatic amino acids. Many of the aromatic hydrocarbons also exhibit a prominent carbon-carbon vibrational stretch between 1346 and 1401 cm^{-1} and one has a strong band at 1296 cm^{-1}. While only one carboxylic acid not dominated by aromatics was examined, it displays a prominent peak between 1424 and 1445 cm^{-1} due to carbon-oxygen stretching, as well as a secondary band at 1283 cm^{-1} from vibrational deformation of methylene. Amino acids lacking benzene ring modes all exhibit a peak between 1311 and 1321 cm^{-1} that can be assigned to the asymmetric rocking of ammonia. Two of these amino acids also have strong bands between 1408 and 1422 cm^{-1} consistent with the stretching of carbon-oxygen bonds in their carboxylate ions. For the inorganic compounds, prominent bands can be attributed to stretching of the sulfate ion (984–1041 cm^{-1}), carbonate ion (1089–1099 cm^{-1}), phosphate ion (962–965 cm^{-1}), nitrate ion (1042–1072 cm^{-1}), and perchlorate ion (935 cm^{-1}). It is important to note that the discrete separation between organic and inorganic features is a potentially powerful discriminator that can be used to triage samples in the field or during planetary missions. Individual spectra and their peak assignments are discussed in more detail below.

4.2.1. Organic standards

Raman spectra for pure organic compounds examined in this study are shown in Fig. 4, and, to the best of our knowledge, this is the first time deep UV Raman spectra of many of these compounds, in the solid phase, have been reported in the literature, and the first time any have been reported at this excitation wavelength. Prominent bands and their assignments are summarized in Fig. 3 and Table 2. Most of the aromatic hydrocarbons have peaks that can be assigned to benzene ring stretching modes at around 1600 cm^{-1} (Lin-Vien et al., 1991; Asher, 1984; Loppnow et al., 2004). Biphenyl, naphthalene, anthracene, phenanthrene, and pyrene all show bands at ~1604 cm^{-1}, ~1632 cm^{-1}, ~1632 cm^{-1}, ~1610 cm^{-1}, and ~1628 cm^{-1}, respectively. Perylene also has a possible weak peak at ~1593 cm^{-1}. These bands are due to the

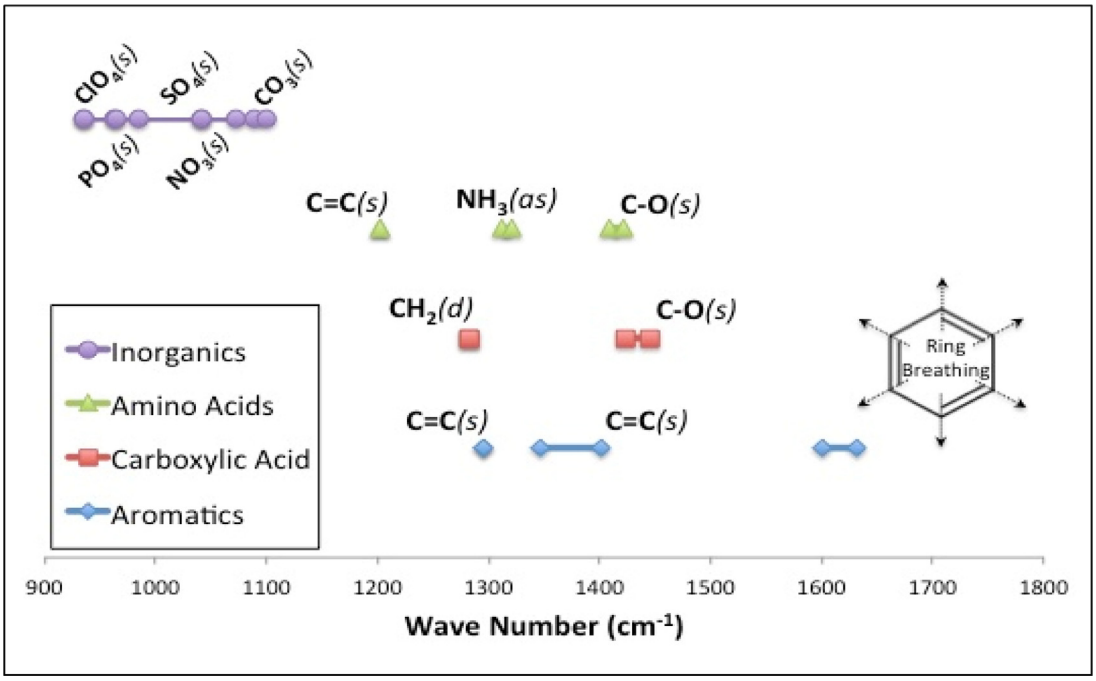

Fig. 3. Prominent deep UV spectral bands (248.6 nm) and their assignments for the aromatics, carboxylic acids, amino acids and inorganics examined in this study. Assignments for bands are indicated for benzene rings (C=C), carbon-oxygen bonds (C–O), methylene groups (CH_2), and ammonia (NH_3), as well as the sulfate (SO_4), carbonate (CO_3), phosphate (PO_4), nitrate (NO_3) and perchlorate (ClO_4) ions. Band assignments are summarized in Tables 2 & 3. *(s)* symmetric stretch; *(d)* vibrational deformation; *(as)* asymmetric rocking.

Table 2
Prominent deep UV Raman bands and assignments for solid phase organic compounds.

Class	Species	SNR[a]	Bands (Cm^{-1})	Assignment	References
Aromatic Hydrocarbons	Biphenyl	95:1	1604	C=C stretching	Lin-Vien et al. (1991); Asher (1984); Loppnow et al. (2004)
	Naphthalene	70:1	1384	C=C stretching	Loppnow et al. (2004)
			1632	C=C stretching	Lin-Vien et al. (1991); Asher (1984); Loppnow et al. (2004)
	Anthracene*	30:1	1401	C=C stretching	Loppnow et al. (2004)
			1632	C=C stretching	Lin-Vien et al. (1991); Asher (1984); Loppnow et al. (2004)
	Phenanthrene*	20:1	1346	C=C stretching	Loppnow et al. (2004)
			1610	C=C stretching	Lin-Vien et al. (1991); Asher (1984); Loppnow et al. (2004)
	Pyrene	110:1	1628	C=C stretching	Lin-Vien et al. (1991); Asher (1984; Loppnow et al. (2004)
	Perylene	30:1	1296	C=C stretching	Socrates (2001)
			1370	C=C stretching	Loppnow et al. (2004)
Carboxylic Acids	Palmitic Acid*	820:1	1283	CH_2 bending	Socrates (2001)
			1424–1445	C–O stretching & O–H bending	Socrates (2001)
	Phthalic Acid	15:1	1601	C=C stretching	Osterrothova and Jehlicka (2010)
	Mellitic Acid	10:1	1608	C=C stretching	Osterrothova and Jehlicka (2010)
			1685	COOH stretching (?)	Jehlicka et al. (2006)
Amino Acids	Glycine*	8580:1	1321	NH_3 rocking	Zhu et al. (2011)
			1408	COO stretching	Zhu et al. (2011)
	Serine	1690:1	1320	NH_3 rocking	Zhu et al. (2011)
			1422	COO stretching	Zhu et al. (2011)
	Histidine*	34,320:1	1264	NCH, CCH	Socrates (2001); Zhu et al. (2011)
			1311	NH_3 rocking	Zhu et al. (2011)
	Tyrosine	45:1	1202	C=C stretching	Rava and Spiro (1985)
			1617	C=C stretching	Jenkins et al. (2005); Zhu et al. (2011)
	Tryptophan	25:1	1623	C=C stretching	Jenkins et al. (2005); Zhu et al. (2011)

SNR has been adjusted accordingly (x3) for the sake of comparison
* compounds used to spike MMS Dust samples at the ~1 wt% level (note: phenanthrene also examined at the ~0.1 wt% level)
[a] signal-to-noise ratios (SNRs) given for the most prominent peaks - note that histidine spectra were collected with only a 10 sec acquisition time (vs 30 sec for other spectra) due to its exceptionally high signal strength; histidine

symmetric stretching and contracting of the carbon-carbon bonds (C=C) in the benzene ring, sometimes referred to as "ring breathing" modes. In addition, naphthalene, anthracene, phenanthrene, and perylene exhibit prominent C=C vibrational stretches at ~1384 cm^{-1}, ~1401 cm^{-1}, ~1346 cm^{-1}, and ~1370 cm^{-1}, respectively (Loppnow et al., 2004). Perylene also has a strong band at ~1296 cm^{-1} that corresponds to the symmetric stretching of benzene (Socrates, 2001). Palmitic acid, a carboxylic acid, displays its most prominent peak between 1424 and 1445 cm^{-1} due to a combination of carbon-oxygen (C–O) stretching and oxygen-hydrogen (O–H) deformation, as well as a secondary band at ~1283 cm^{-1} due to the vibrational deformation of methylene (CH_2), a common vibrational feature in long-chain aliphatic carboxylic acids, normally quite weak under visible excitation (Socrates, 2001).

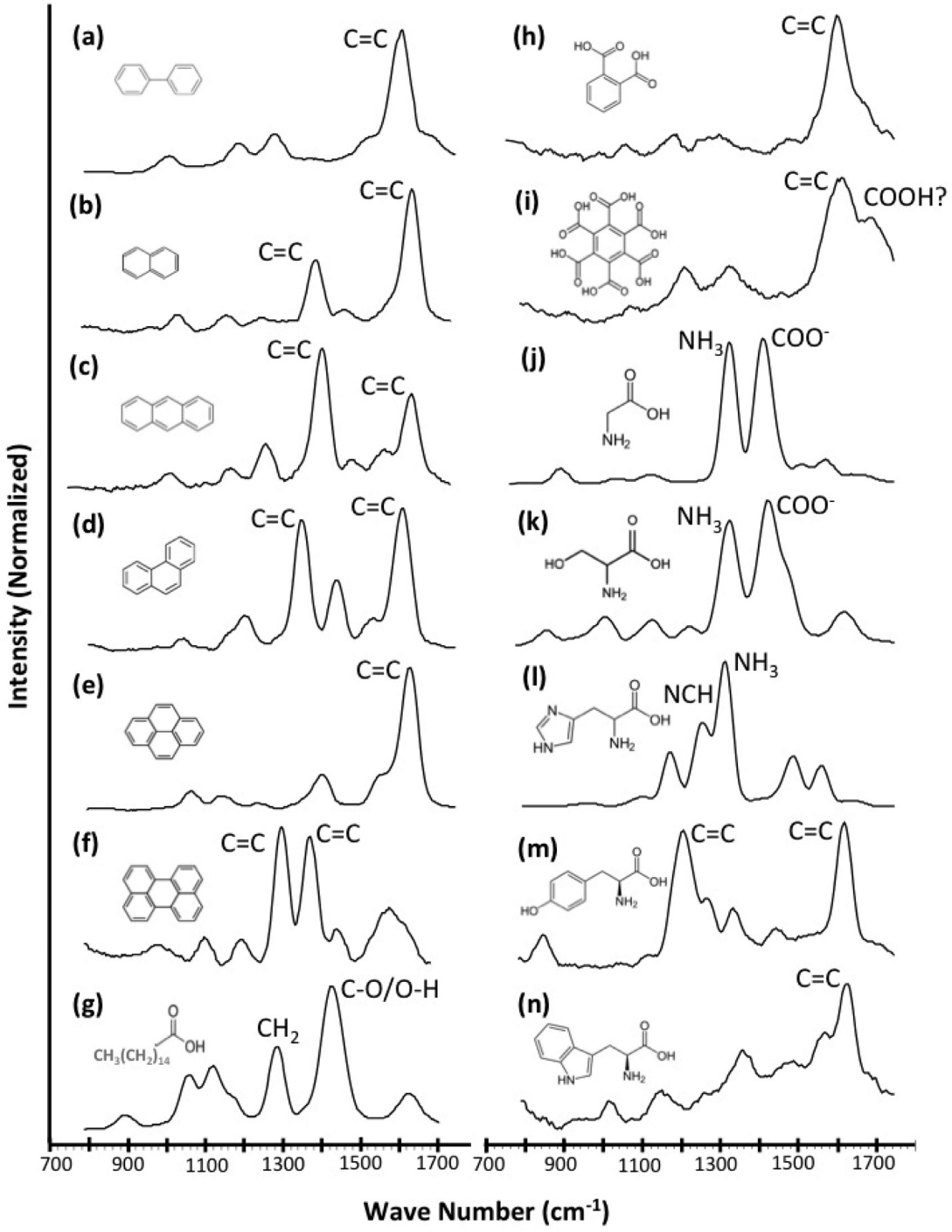

Fig. 4. Deep UV Raman spectra (248.6 nm) of solid phase organic compounds, in granular or powdered form, as described in Table 1: (a) biphenyl, (b) naphthalene, (c) anthracene, (d) phenanthrene, (e) pyrene, (f) perylene, (g) palmitic acid, (h) phthalic acid, (i) mellitic acid, (j) glycine, (k) serine, (l) histidine, (m) tyrosine, and (n) tryptophane. Assignments for prominent bands are indicated for benzene rings (C=C), carbon-oxygen bonds (C–O), oxygen-hydrogen bonds (O–H), methylene groups (CH_2), carboxyl groups (COOH), ammonia (NH_3), carboxylate ions (COO^-), and imidazole group (NCH). Spectra were collected using a 30 sec acquisition time and a 40 Hz pulse rate (N = 5 per sample, 4 for those marked ()). Note that histidine spectra were collected with only a 10 sec acquisition time due to its exceptionally high signal strength, as greater acquisition times tended to saturate the detector. Individual spectra normalized to strongest peak and stacked for comparison. Prominent bands and their assignments are summarized in Fig. 3 and Table 2.

In contrast, phthalic and mellitic acid show prominent peaks at ~1601 cm^{-1} and ~1608 cm^{-1}, respectively, indicative of C=C or benzene ring stretching (Osterrothova and Jehlicka, 2010). Mellitic acid also has a potential band at ~1685 cm^{-1}, on the shoulder of the C=C peak, that may correspond to the asymmetric stretching of the carboxyl molecule (COOH) (Jehlicka et al., 2006). Glycine, serine, and histidine, amino acids, all have peaks that can be assigned to the asymmetric rocking of ammonia (NH_3) at ~1321 cm^{-1}, ~1320 cm^{-1}, and ~1311 cm^{-1}, respectively (Zhu et al., 2011). Glycine and serine also have strong bands at ~1408 cm^{-1} and ~1422 cm^{-1}, respectively, consistent with symmetric stretching of the carboxylate ion (COO^-), and histidine has a prominent peak at ~1264 cm^{-1} corresponding to its imidazole (NCH) group (Zhu et al., 2011). The aromatic amino acids, tyrosine and

Table 3
Prominent deep UV Raman bands and assignments for solid phase inorganic compounds.

Class	Species	SNR[a]	Bands (cm^{-1})	Assignment	References
Sulfate Minerals	Gypsum*	1720:1	1009	SO_4 stretching	Berenblut et al. (1971); Wang et al. (2006); Chio et al. (2007)
	Mg-hydrated sulfates	440:1	1041	SO_4 stretching	Berenblut et al. (1971); Wang et al. (2006); Chio et al. (2007)
	Fe-hydrated sulfates	20:1	984	SO_4 stretching	Berenblut et al. (1971); Wang et al. (2006); Chio et al. (2007)
Carbonate Minerals	Calcite	705:1	1089	CO_3 stretching	Rividi et al. (2010)
	Magnesite*	360:1	1094	CO_3 stretching	Rividi et al. (2010)
	Ankerite–Dolomite	30:1	1099	CO_3 stretching	Rividi et al. (2010)
Phosphate Minerals	Fluorapatite*	30:1	965	PO_4 stretching	Boyer and Fleury (1974)
	Chlorapatite	25:1	962	PO_4 stretching	Boyer and Fleury (1974)
Nitrates	NH_4-nitrate	450:1	1042	NO_3 stretching	Rousseau et al. (1968); Misra et al. (2010)
	Na-nitrate	2645:1	1072	NO_3 stretching	Rousseau et al. (1968); Misra et al. (2010)
	K-nitrate*	860:1	1051	NO_3 stretching	Rousseau et al. (1968); Misra et al. (2010)
Perchlorates	K-perchlorate*	1125:1	935	ClO_4 stretching	Gu et al. (2009)

* compounds used to spike MMS Dust samples at the ~1 wt% level
[a] signal-to-noise ratios (SNRs) given for the most prominent peaks

tryptophan, like the aromatic hydrocarbons, have peaks consistent with the presence of C=C or ring stretching at ~1617 cm^{-1} and ~1623 cm^{-1}, respectively (Jenkins et al., 2005; Zhu et al., 2011). Tyrosine has an additional band at ~1202 cm^{-1} that also corresponds to the symmetric stretching of benzene (Rava and Spiro, 1985).

When examining the spectra in Fig. 4, it becomes readily apparent that many of the organic compounds analyzed in this study exhibit very high signal-to-noise ratios (SNRs; see Table 2). Non-aromatic compounds, like histidine (SNR = 34320:1), glycine (SNR = 8580:1), serine (SNR = 1690:1), and palmitic acid (SNR = 820:1), all have signal strengths orders of magnitude greater than most of the organics considered in this study. When compared to the lower signal strengths for compounds with aromatic features, like tyrosine (SNR = 45:1), tryptophan (SNR = 25:1), phthalic acid (SNR = 15:1), and mellitic acid (SNR = 10:1), as well as the aromatic hydrocarbons (SNRs = 20:1 to 110:1), the assumption could be made that non-aromatic structures have a higher Raman cross section than aromatic features. However, aromatic structures are well known for having high molecular absorptivities in the UV spectral region, as well as commonly exhibiting resonance enhancement effects when excited at UV wavelengths (Frosch et al., 2007; Tarcea et al., 2007; Bhartia et al., 2008), so one would expect the aromatic compounds to exhibit *stronger* signals than the non-aromatic compounds. This disparity is due to the fact that aromatic compounds are highly absorptive at these wavelengths and absorb more of the scattered Raman photons, which constitutes the Raman signal, limiting the number of photons observed when samples are examined in bulk (Wu et al., 2006). This effect is most obvious when looking at pure samples, where sensitivity appears low even though the interaction volume is completely filled with the compound being interrogated. Despite this effect, highly absorbing materials, such as the aromatic hydrocarbons, are more amenable than other compounds to trace detection, such as when materials are dispersed in a background matrix or are present as a thin layer on or in a substrate. This effect is demonstrated and will be discussed in more detail below in Section 4.3.

4.2.2. Inorganic standards

Raman spectra for inorganic compounds examined in this study are shown in Fig. 5, and, to the best of our knowledge, this is the first time model spectra for these compounds have been reported in the literature at this excitation wavelength. Prominent bands and their assignments are summarized in Fig. 3 and Table 3. All of these minerals and compounds contain biologically important elements (C, H, N, O, P, S) and, as such, their abundance and diversity in a sedimentary environment are key measures of habitability. On Earth, life is driven by oxidation–reduction (redox) reactions that form and transform organic matter, as well as compounds that contain these key elements, such as sulfates, carbonates, phosphates, and nitrates. Perchlorates on the other hand, due to their oxidative nature, are generally harmful to life, but this is also an important part of the habitability equation. The presence of any of these compounds, especially in association with organic matter, or when their presence implies some degree of chemical and/or morphologic disequilibrium, is an important component in the evaluation of biogenicity. Gypsum, as well as the Mg- and Fe-hydrated sulfates, exhibit primary peaks at ~1009 cm^{-1}, ~1041 cm^{-1}, and ~984 cm^{-1}, respectively, consistent with the fundamental vibrational mode of the sulfate (SO_4) tetrahedron (Berenblut et al., 1971; Wang et al., 2006; Chio et al., 2007). Similarly, calcite, magnesite, and ankerite-dolomite, all have prominent peaks at ~1089 cm^{-1}, ~1094 cm^{-1}, and ~1099 cm^{-1}, respectively, due to the symmetric vibrational stretch in the carbonate (CO_3) trigonal plane (Rividi et al., 2010). Fluorapatite and chlorapatite have peaks at ~965 cm^{-1} and 962 cm^{-1}, respectively, as a result of the symmetric vibrational stretch of the phosphate (PO_4) molecule (Boyer and Fleury, 1974). NH_4-, Na-, and K-nitrate all exhibit prominent peaks at ~1042 cm^{-1}, ~1072 cm^{-1}, and ~1051 cm^{-1}, respectively, due to the symmetric stretching mode of the nitrate (NO_3) ion (Rousseau et al., 1968; Misra et al., 2010). And K-perchlorate has a primary peak at ~935 cm^{-1} attributed to the symmetric stretching of the perchlorate (ClO_4) ion (Gu et al., 2009). The lower bound on the spectral range in this study is hindered by current deep UV filter technology and limits detecting certain classes of minerals that exhibit spectral features below 750 cm^{-1} (e.g., some silicates); however, it is our intention to demonstrate a range that highlights detection of organic compounds as well as key inorganic compounds of astrobiological interest.

4.3. Analysis of MMS + 1 wt% standards

In order to evaluate how well these organic and inorganic compounds can be resolved under natural 'real world' conditions (matrix effects, etc) we spiked samples of the MMS analog with ~1 wt% each of standards representative of the major classes of compounds presented in Table 1. In addition to bands native to the MMS, the spectra in Fig. 6 reveal peaks consistent with the spiked compounds. Anthracene and phenanthrene both have strong C=C ring breathing modes at 1401 cm^{-1} and 1349 cm^{-1}, respectively, while phenanthrene demonstrates an additional C=C stretch at 1609 cm^{-1}. Palmitic acid is characterized by a combination of C–O stretching and O–H deformation at 1445 cm^{-1}. And both glycine and histidine have bands at 1324 cm^{-1} and 1327 cm^{-1}, respectively, that can be assigned to the rocking of NH_3, while glycine also displays COO^- symmetric stretching at

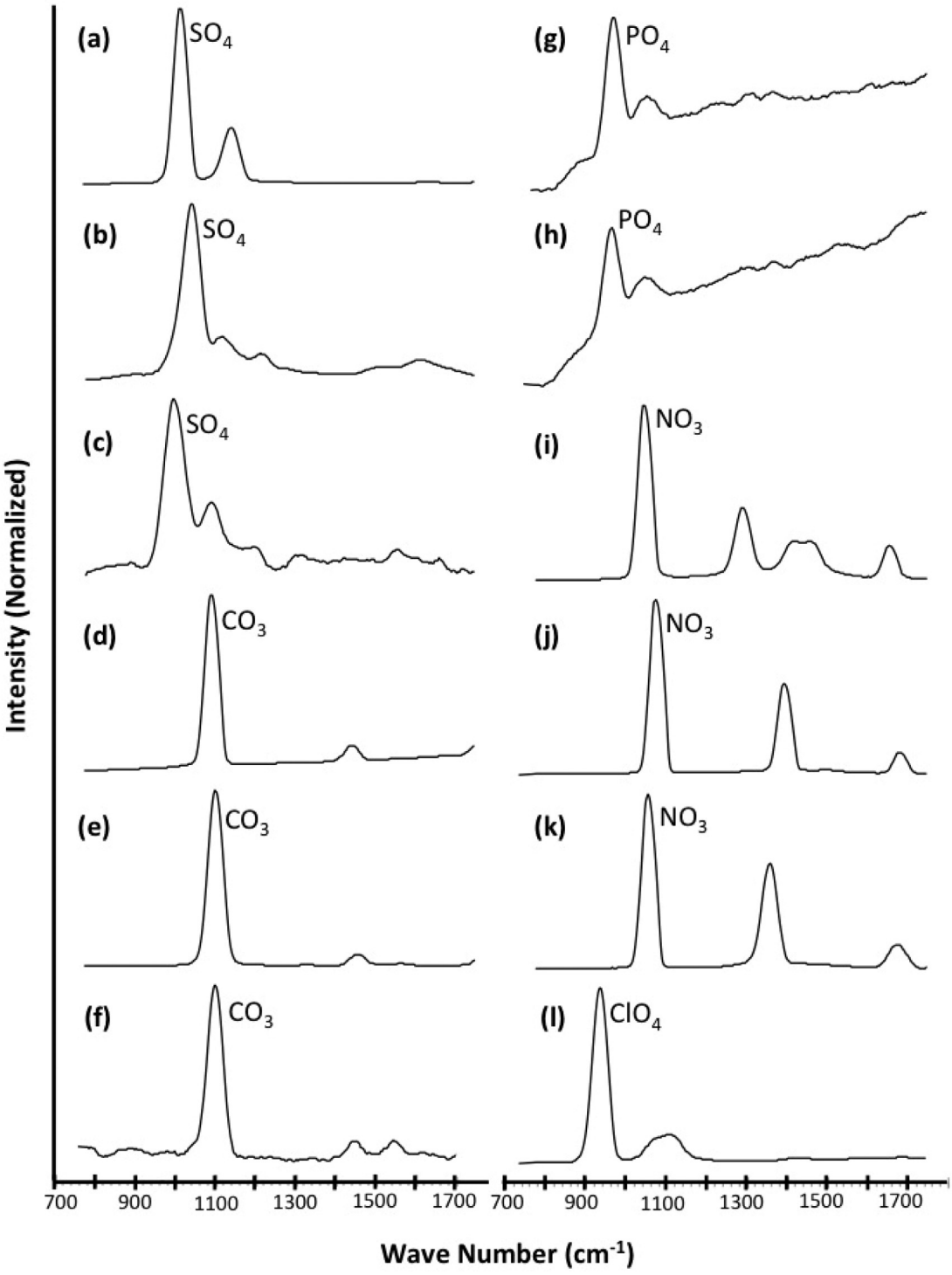

Fig. 5. Deep UV Raman spectra (248.6 nm) of solid phase inorganic compounds, in granular or powdered form, as described in Table 1: (a) gypsum, (b) Mg-hydrated sulfate, (c) Fe-hydrated sulfate*, (d) calcite, (e) magnesite, (f) ankerite-dolomite, (g) fluorapatite, (h) chlorapatite, (i) NH_4-nitrate, (j) Na-nitrate, (k) K-nitrate, (l) K-perchlorate. Assignments for prominent bands are indicated for sulfate (SO_4), carbonate (CO_3), phosphate (PO_4), nitrate (NO_3), and perchlorate (ClO_4) molecules. All spectra were collected using a 30 sec acquisition time and a 40 Hz pulse rate (N = 2 per sample, 5 for those marked (*)). Individual spectra normalized to strongest peak and stacked for comparison. Prominent bands and their assignments are summarized in Fig. 3 and Table 3.

1406 cm^{-1} and histidine displays a prominent peak at 1271 cm^{-1} representing its imadazole group (NCH). Gypsum and magnesite show primary peaks at 1006 cm^{-1} and 1095 cm^{-1}, representing symmetric stretching of SO_4 and CO_3, respectively, however, given that both of these compounds are natively present in the MMS, caution should be exercised before any conclusions can be made, though in both cases, there does appear to be an increase in signal strength above the native background levels. Finally, fluorapatite, K-nitrate, and K-perchlorate have bands at 966 cm^{-1}, 1054 cm^{-1}, and 936 cm^{-1}, that can be assigned to vibration of the PO_4, NO_3, and ClO_4 ions, respectively.

When examining spectra in Fig. 6, it is apparent that the aromatic compounds, anthracene (SNR = 180:1) and phenanthrene (SNR = 124:1), exhibit signal-to-noise ratios significantly higher

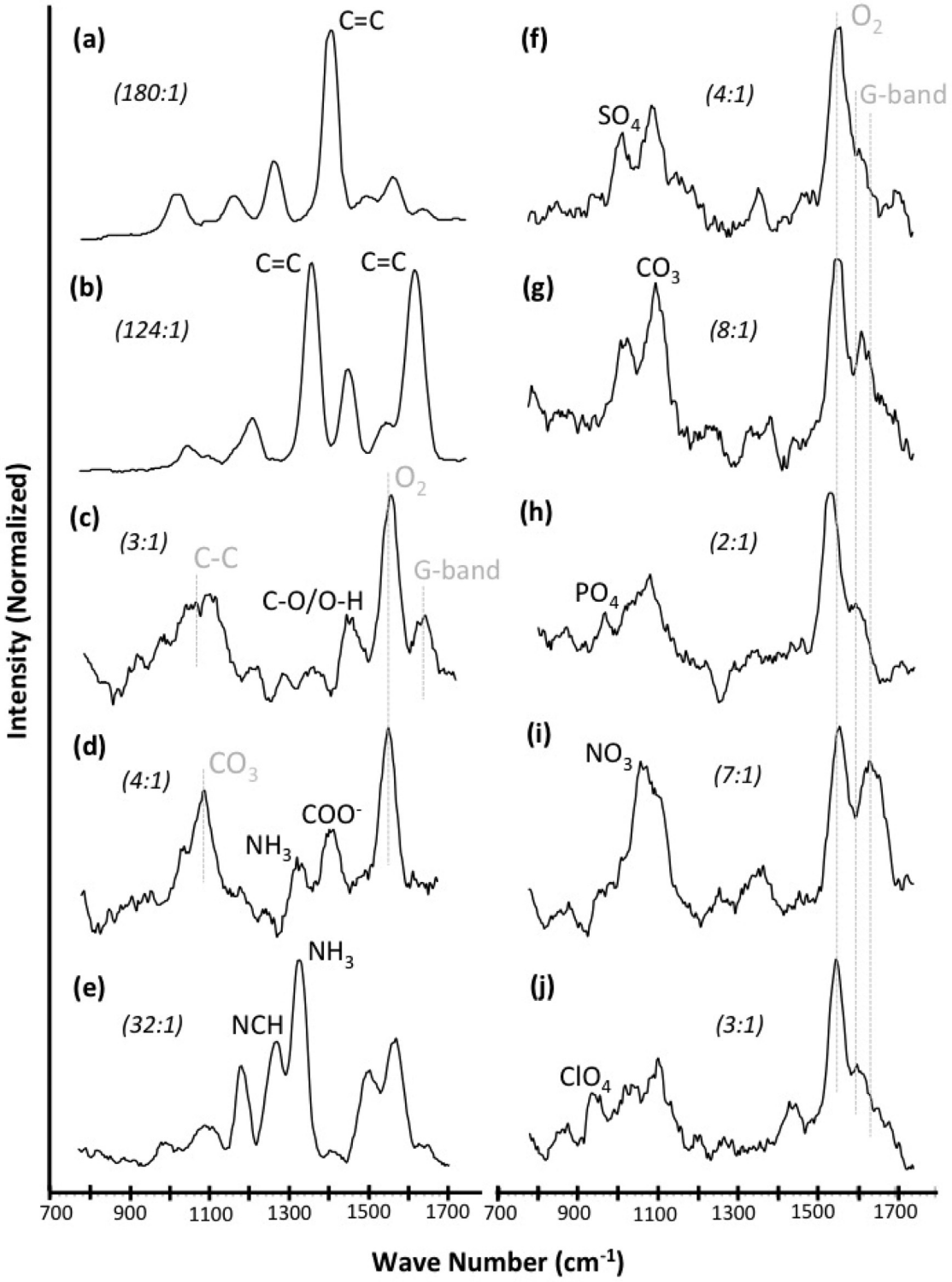

Fig. 6. Deep UV Raman spectra (248.6 nm) of the Mojave Mars Simulant (MMS) Dust, in pellet form, spiked with a) 1.04 wt% anthracene, b) 1.01 wt% phenanthrene, c) 0.99 wt% palmitic acid, d) 1.51 wt% glycine, e) 0.94 wt% histidine, f) 1.03 wt% gypsum, g) 1.16 wt% magnesite, h) 1.05 wt% fluorapatite, i) 1.10 wt% K-nitrate, and j) 1.11 wt% K-perchlorate, showing bands native to the MMS (in gray), as well as those consistent with spiked material. Signal-to-noise ratios (SNRs) for peaks diagnostic of these contaminants are given in parentheses. Spectra were collected using a 300 sec 'moving average' (see Methods) and a 20 Hz pulse rate. Individual spectra normalized to strongest peak and stacked for comparison.

than the other compounds evaluated (SNRs = 2:1 to 32:1). This may seem counter-intuitive when contrasting these results to those of the bulk standards in Figs. 4 and 5, where the aromatic compounds can be seen to have lower signal strength relative to other compounds (see Tables 2 and 3). However, as mentioned above in Section 4.2.1, the higher molecular absorptivities of the aromatic hydrocarbons allow fewer molecules to be detected in bulk samples when increased signal strength is the result of resonance effects. In situations where the concentration is higher, these compounds will be inhibited or dampened by self-absorption

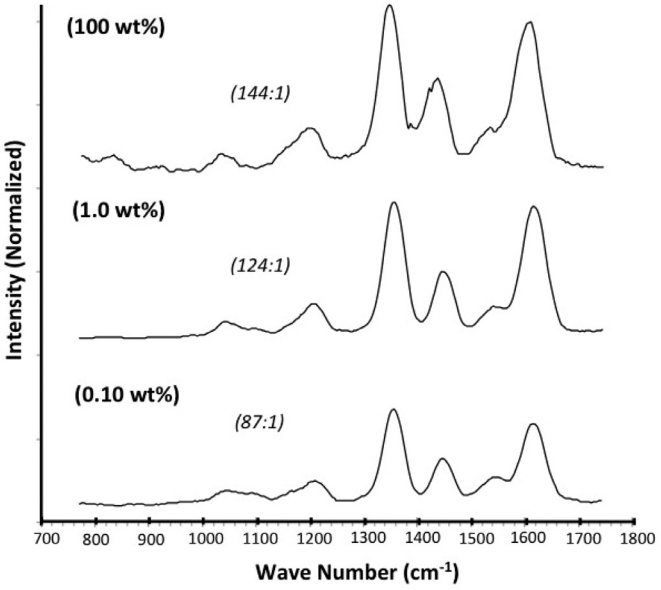

Fig. 7. Deep UV Raman spectra (248.6 nm) of 100 wt% phenanthrene, in pellet form, and Mojave Mars Simulant (MMS) Dust, also in pellet form, spiked with 1.01 wt% and 0.10 wt% phenanthrene. Signal-to-noise ratios (SNRs) for the most prominent peaks are given in parentheses. Spectra were collected using a 300 sec 'moving average' (see methods) and a 20 Hz pulse rate. All spectra normalized to the strongest peak of the 100 wt% sample and stacked for comparison.

(Wu et al., 2006). This leads to an interesting phenomenon where interrogation of a pure sample may not yield a significantly better response than interrogation of a sample containing only 1 wt% of a given compound. To demonstrate this further, we examined three samples of phenanthrene with concentrations ranging from 100 wt% for pure phenanthrene to ~1 wt% and ~0.1 wt% for phenanthrene mixed with the MMS analog. As can be seen in Fig. 7, there is only a 14% decrease in signal strength when going from 100 wt% to 1 wt% phenanthrene (SNRs = 144:1 & 124:1, respectively). In addition, going from 1 wt% to 0.1 wt% phenanthrene only results in a 30% drop in signal strength despite an order of magnitude decrease in concentration (SNRs = 124:1 & 87:1, respectively). In weakly or non-absorbing compounds a linear decrease as a function of decreasing concentration would be expected, but the data for phenanthrene defines a natural log function with decreasing concentration. This shows that for highly absorbing materials, such as aromatic compounds, deep UV excitation offers an advantage for detecting lower concentrations of particles, which is particularly useful when examining natural or 'real world' samples where trace levels of in situ organic compounds may be dispersed throughout a soil or regolith.

5. Conclusions

We demonstrate that Raman scattering from deep UV excitation is capable of detecting a wide variety of organics and astrobiologically relevant minerals dispersed throughout a Mars relevant matrix. Compared to excitation by visible, near IR, or IR based methods, where the mineral transparency is higher, deep UV excitation has a smaller interaction depth; however, as demonstrated using analog materials spiked with organics, the Raman scattering effect is still detectable down to at least 1 wt% or even 0.1 wt% for certain materials. This is made possible for two reasons: 1) the Raman effect is enhanced by lower wavelength excitation per the Rayleigh Law, and, for organics with aromatic or conjugated bonds, resonance enhancement effects; and 2) since background fluorescence does not contaminate the Raman region with deep UV excitation, the small diameter illumination beams used in traditional laboratory spectroscopy to mitigate fluorescence can be increased by an order of magnitude, increasing the interaction volume by 100 to 1000x, and increasing the sampling density by > 1000x, making it highly suitable to searching for organics on surfaces where the location may not be readily apparent from color or surface texture alone.

In addition, these data form the basis of a signal-to-noise model for SHERLOC and other future fieldable instrumentation incorporating deep UV Raman spectroscopy. An extension of this is a laboratory tool that enables spatially resolved organic detection and analysis without loss of spatial context; a method that when coupled to other mineral, elemental, and morphological imaging modalities, can be used to assess the provenance of abiotic organics and understand microbial-mineral interaction. However, while location and context can be assessed, the phenanthrene concentration experiment highlights self-absorption is a confounding effect when deciphering concentration. To derive an accurate sample concentration using deep UV Raman spectroscopy not only requires a concentration response curve, but also knowledge of molecular absorptions for the detected species, as well as their interaction volume. These additional parameters are difficult to assess on a natural surface, but will be the focus of future research.

Acknowledgments

This work was carried out at the Jet Propulsion Laboratory, California Institute of Technology under a contract with the National Aeronautics and Space Administration. Government sponsorship acknowledged. Funding for this work was provided by the NASA Astrobiology Institute (NAI Life Underground Publication NNA13AA92A) and NASA Astrobiology Science and Instrument Development (GURILA NNH10ZDA001N). This is an NAI-Life Underground Publication Number 100. The authors would like to thank Dr. Evan Eshelman for helpful discussions. We also greatly appreciate comments from Prof. Alexis Templeton and an anonymous reviewer which immeasurably improved this manuscript.

References

Adcock, C.T., Hausrath, E.M., Forster, P.M., 2013. Readily available phosphate from minerals in early aqueous environments on Mars. Nat. Geosci. 6 (10), 824–827.
Alajtal, A.I., Edwards, H.G.M., Scowen, I.J., 2010. Raman spectroscopic analysis of minerals and organic molecules of relevance to astrobiology. Anal. Bioanal. Chem. 397, 215–221.
Albrecht, A.C., Hutley, M.C., 1971. Dependence of vibrational Raman intensity on wavelength of incident light. J. Chem. Phys. 55 (9), 4438–4443.
Anderson, R.C., Beegle, L.W., Peters, G.H., Fleming, G.M., Jandura, L., Kriechbaum, K., Manatt, K., Okon, A., Pounders, E., Sollitt, L., Sunshine, D., 2009. Particle transport and distribution on the Mars science laboratory mission: effects of triboelectric charging. Icarus 204 (2), 545–557.
Asher, S.A., 1984. Ultraviolet resonance Raman spectrometry for detection and speciation of trace polycyclic aromatic hydrocarbons. Anal. Chem. 56, 720–724.
Asher, S.A., 1988. UV resonance Raman studies of molecular-structure and dynamics - applications in physical and biophysical chemistry. Annu. Rev. Phys. Chem. 39, 537–588.
Asher, S.A., 1993. UV resonance Raman spectroscopy for analytical, physical, and biophysical chemistry, part 2. Anal. Chem. 65 (4), 201–210.
Asher, S.A., Johnson, C.R., 1984. Raman-spectroscopy of a coal liquid shows that fluorescence Interference is minimized with ultraviolet excitation. Science 225, 311–313 (4659).
Asher, S.A., Ludwig, M., Johnson, C.R., 1986. UV resonance Raman excitation profiles of the aromatic amino acids. J. Am. Chem. Soc. 108 (12), 3186–3197.
Bandfield, J.L., Glotch, T.D., Christensen, P.R., 2003. Spectroscopic identification of carbonate minerals in the Martian dust. Science 301, 1084–1087 (5636).
Becker, L., Popp, B., Rust, T., Bada, J.L., 1999. The origin of organic matter in the Martian meteorite ALH84001. Adv. Sp. Res. 24 (4), 477–488.
Beegle, L.W., Anderson, R.C., Fleming, G.M., 2010. Understanding cross sample contamination in sample handling systems on Mars: effects of tribophysical charging. Astrobiology Science Conference 2010. Abstract # 5208.
Beegle, L.W., Bhartia, R., DeFlores, L., Darrach, M., Kidd, R.D., et al., 2014. SHERLOC: scanning habitable environments with Raman and luminescence for organic and chemicals, an investigation for 2020. Abstract #1777 Presented at the 45th Lunar and Planetary Science Conference.

Beegle, L.W., Bhartia, R., White, M., DeFlores, L., Abbey, W., et al., 2015. SHERLOC: scanning habitable environments with Raman and luminescence for organic and chemicals. In: 2015 IEEE Aerospace Conference, pp. 1–11. doi:10.1109/AERO.2015.7119105.

Benner, S.A., Devine, K.G., Matveeva, L.N., Powell, D.H., 2000. The missing organic molecules on Mars. Proc. Nation. Acad. Sci. 97 (6), 2425–2430.

Berenblut, B.J., Dawson, P., Wilkinson, G.R., 1971. The Raman spectrum of gypsum. Spectrochimica Acta Part A 27 (9), 1849–1863.

Bhartia, R., Hug, W.F., Salas, E.C., Reid, R.D., Sijapati, K.K., Tsapin, A., Abbey, W., Nealson, K.H., Lane, A.L., Conrad, P.G., 2008. Classification of organic and biological materials with deep ultraviolet excitation. Appl. Spectrosc. 62 (10), 1070–1077.

Bhartia, R., Salas, E.C., Hug, W.F., Reid, R.D., Lane, A.L., Edwards, K.J., Nealson, K.H., 2010. Label-free bacterial imaging with deep-UV-laser-induced native fluorescence. Appl. Env. Microbiol. 76 (21), 7231–7237.

Bhartia, R., Hug, W.F., Reid, R., Salas, E.C. 2012a. Non-contact, reagentless, nondestructive, detection of organics, biosignatures, and water. SPIE Defense 83850E-83850E-9. doi:10.1117/12.921420.

Bhartia, R., Hug, W.F., DeFlores, L.P., Fries, M.D., Reid, R.D., Allwood, A., Abbey, W., Salas, E.C., Beegle, L., 2012b. Finding the organics: a compact non-contact, non-invasive trace organic and mineralogical mapping arm instrument. LPI Contrib. 1679, 4188. http://adsabs.harvard.edu/abs/2012LPICo1679.4188B.

Biemann, K., Lavoie, J.M., 1979. Some final conclusions and supporting experiments related to the search for organic-compounds on the surface of Mars. J. Geophys. Res. 84, 8385–8390.

Botta, O., Bada, J.L., 2002. Extraterrestrial organic compounds in meteorites. Surv. Geophys. 23 (5), 411–467.

Boyer, L.L., Fleury, P.A., 1974. Determination of interatomic interactions in $Ca_{10}(PO_4)_6F_2$ (fluorapatite) from structural and lattice-dynamical data. Phys. Rev. B 9 (6), 2693–2700.

Boynton, W.V., Bailey, S.H., Hamara, D.K., Williams, M.S., Bode, R.C., et al., 2001. Thermal and evolved gas analyzer: part of the Mars volatile and climate surveyor integrated payload. J. Geophys. Res. Planets 106 (E8), 17683–17698 (1991-2012).

Boynton, W.V., Ming, D.W., Kounaves, S.P., Young, S.M.M., Arvidson, R.E., Hecht, M.H., Hoffman, J., Niles, P.B., Hamara, D.K., Quinn, R.C., Smith, P.H., Sutter, B., Catling, D.C., Morris, R.V., 2009. Evidence for calcium carbonate at the Mars Phoenix landing site. Science 325, 61–64 (5936).

Bozlee, B.J., Misra, A.K., Sharma, S.K., Ingram, M., 2005. Remote Raman and fluorescence studies of mineral samples. Spectrochimica Acta Part A 61 (10), 2342–2348.

Bruker, AXS., 2007. DIFFRAC^{plus} EVA 13 Basic Evaluation Package - Release 2007. Bruker AXS, Karlsruke, Germany.

Bruker, AXS., 2008. TOPAS V. 4: General Profile and Structure Analysis Software for Powder Diffraction Data. Bruker AXS, Karlsruke, Germany.

Burris, J., McGee, T.J., Heaps, W., 1992. UV Raman cross section in nitrogen. Appl. Spectrosc. 46 (6), 1076.

Carter, D.A., Pemberton, J.E., 1995. Frequency/wavelength calibration of multipurpose multichannel Raman spectrometers. part i: instrumental factors affecting precision. Appl. Spectrosc. 49 (11), 1550–1560.

Chadha, S., Manoharan, R., Moenne-Locooz, P., Nelson, W.H., Peticolas, W.L., Sperry, J.F., 1993. Comparison of the UV resonance Raman spectra of bacteria, bacteria cell walls and ribosomes excited in the deep UV. Appl. Spectrosc. 47 (1), 38–43.

Cheary, R.W., Coelho, A.A., 1992. A fundamental parameters approach to X-ray line-profile fitting. J. Appl. Crystallogr. 25, 109–121.

Chio, C.H., Sharma, S.K., Muenow, D.W., 2007. The hydrates and deuterates of ferrous sulfate ($FeSO_4$): a Raman spectroscopic study. J. Raman Spectrosc. 38 (1), 87–99.

Chu, P.K., Li, L., 2006. Characterization of amorphous and nanocrystalline carbon films. Mater. Chem. Phys. 96, 253–277.

Chung, F.H., 1974. Quantitative interpretation of X-ray diffraction patterns of mixtures. II. Adiabatic principle of X-ray diffraction analysis of mixtures. J. Appl. Crystallogr. 7, 526–531.

Clegg, S.M., Wiens, R.C., Maurice, S., Gasnault, O., Forni, O., Sharma, S.K., Misra, A.K., Rull, F., Johnson, J.R. 2014. Abstract #P11A-3753 presented at the American Geophysical Union, Fall Meeting 2014.

Dibblee, T.W., 1958. Tertiary Stratigraphic Units of Western Mojave Desert. American Association of Petroleum Geologists Bulletin, California, pp. 135–144. 42.

Dibblee, T.W., 1967. Areal Geology of the Western Mojave Desert California. United States Government Printing Office, Washington, D.C.

Ehlmann, B.L., Mustard, J.F., Murchie, S.L., Poulet, F., Bishop, J.L., Brown, A.J., Calvin, W.M., Clark, R.N., Des Marais, D.J., Milliken, R.E., Roach, L.H., Roush, T.L., Swayze, G.A., Wray, J.J., 2008. Orbital identification of carbonate-bearing rocks on Mars. Science 322, 1828–1832 (5909).

Ehlmann, B.L., Edwards, C.S., 2014. Mineralogy of the Martian surface. Annu. Rev. Earth Planet. Sci. 42 (1). doi:10.1146/annurev-earth-060313-055024.

Ellery, A., Wynn-Williams, D., 2003. Methodologies and techniques for detecting extraterrestrial (microbial) life: why Raman spectroscopy on Mars? – a case of the right tool for the right job. Astrobiology 3, 565–579.

Eshelman, E., Daly, M.G., Slater, G., Dietrich, P., Gravel, J.F., 2014. Ultraviolet Raman wavelength for the in-situ analysis of organic compounds releveant to astrobiology. Planet. Sp. Sci.. http://dx.doi.org/10.1016/j.pss.2014.01.021.

Ferrari, A.C., Robertson, J., 2000. Interpretation of Raman spectra of disordered and amorphous carbon. Phys. Rev. B 61 (20), 14095–14107.

Ferrari, A.C., Robertson, J., 2001. Resonant Raman spectroscopy of disordered, amorphous, and diamond-like carbon. Phys. Rev. B 64, 075414–1-13. doi:10.1103/PhysRevB.64.075414.

Flynn, G.J., 1996. The delivery of organic matter from asteroids and comets to the early surface of Mars. Earth Moon Planets 72, 469–474.

Freissinet, C., Glavin, D.P., Mahaffy, P.R., Miller, K.E., Eigenbrode, J.L., et al. 2014. Organic molecules in the sheepbed mudstone, gale crater, Mars. Abstract #1349 presented at the 8th International Conference on Mars.

Frosch, T., Tarcea, N., Schmitt, M., Thiele, H., Langenhorst, F., Popp, Jurgen., 2007. UV Raman imaging - a promising tool for astrobiology: comparative Raman studies with different excitation wavelengths on SNC martian meteorites. Anal. Chem. 79 (3), 1101–1108.

Glavin, D.P., Bada, J.L., Brinton, K.L.F., McDonald, G.D., 1999. Amino acids in the Martian meteorite Nakhla. In: Proceedings of the National Academy of Sciences of the United States of America, 96, pp. 8835–8838. doi:10.1073/pnas96.16.8835.

Glavin, D., Freissinet, C., Mahaffy, P., Miller, K., Eigenbrode, J., et al., 2015. Martian chlorobenzene identified by curiosity in yellowknife bay: evidence for the preservation of organics in a mudstone on Mars. Abstract #1178 presented at the 46th Lunar and Planetary Science Conference.

Gilkes, K.W.R., Sands, H.S., Batchelder, D.N., Robertson, J., Milne, W.I., 1997. Direct observations of sp^3 bonding in tetrahedral amorphous carbon using ultraviolet Raman spectroscopy. Appl. Phys. Lett. 70, 1980–1982.

Gu, B., Ruan, C., Wang, W., 2009. Perchlorate Detection at Nanomolar Concentrations by Surface-Enhanced Raman Scattering. Appl. Spectros. 63 (1), 98–102.

Hecht, M.H., Kounaves, S.P., Quinn, R.C., West, S.J., Young, S.M.M., Ming, D.W., Catling, D.C., Clark, B.C., Boynton, W.V., Hoffman, J., DeFlores, L.P., Gospodinova, K., Kapit, J., Smith, P.H., 2009. Detection of perchlorate and the soluble chemistry of Martian soil at the Phoenix lander site. Science 325, 64–67 (5936).

Hill, R.J., Howard, C.J., 1987. Quantitative phase analysis from neutron powder diffraction data using the Rietveld method. J. Appl. Crystallogr. 20, 467–474.

Jehlicka, J., Edwards, H.G.M., Jorge Villar, S.E., 2006. Raman spectroscopic study of mellite - a naturally occurring aluminum benzenehexacarboxylate from lignite - claystone series of the Tertiary age. Spectrochimica Acta Part A 65 (1), 229–234.

Jehlicka, J., Edwards, H.G.M., Vitek, P., 2009. Assessment of Raman spectroscopy as a tool for the non-destructive identification of organic minerals and biomolecules for Mars studies. Planet. Space Sci. 57, 606–613.

Jenkins, A.L., Larsen, R.A., Williams, T.B., 2005. Characterization of amino acids using Raman spectroscopy. Spectrochimica Acta Part A 61, 1585–1594.

Kminek, G., Bada, J.L., 2006. The effect of ionizing radiation on the preservation of amino acids on Mars. Earth Planet. Sci. Lett. 245, 1–5.

Kumamoto, Y., Taguchi, A., Smith, N.I., Kawata, S., 2011. Deep UV resonant Raman spectroscopy for photodamage characterization in cells. Biomed. Opt. Express 2 (4), 927–936.

Ladino, L.A., Abbatt, J.P.D., 2013. Laboratory investigation of Martian water ice cloud formation using dust aerosol simulants. J. Geophys. Res. 118 (1), 14–25.

Leshin, L.A., Mahaffy, P.R., Webster, C.R., Cabane, M., Coll, P., et al., 2013. Volatile, isotope, and organic analysis of martian fines with the Mars Curiosity rover. Science 341 (6153). doi:10.1126/science.1238937.

Lin-Vien, D., Colthup, N.B., Fateley, W.G., Grassell, J.G., 1991. The Handbook of Infrared and Raman characteristic Frequencies of Organic Molecules. Elsevier.

Loppnow, G.R., Shoute, L., Schmidt, K.J., Savage, A., Hall, R.H., Bulmer, J.T., 2004. UV Raman spectroscopy of hydrocarbons. Philos. Trans. R. Soc. London A 362, 2461–2476.

Mahaffy, P.R., Webster, C.R., Cabane, M., Conrad, P.G., Coll, P., et al., 2012. The Sample Analysis at Mars Investigation and Instrument Suite. Space Sci. Rev. 170 (1-4), 401–478.

Manning, C.V., McKay, C.P., Zahnle, K.J., 2008. The nitrogen cycle on Mars: Impact decomposition of near-surface nitrates as a source for a nitrogen steady state. Icarus 197 (1), 60–64.

McCreery, R.L., 2005. Raman Spectroscopy For Chemical analysis.. John Wiley & Sons Inc, New York.

McKay, D.S., Gibson Jr., E.K., Thomas-Keptra, K.L., Vali, H., Romanek, C.S., Clemett, S.J., Chiller, X.D.F., Maechling, C.R., Zare, R.N., 1996. Search for Past Life on Mars: Possible Relic Biogenic Activity in Martian Meteorite ALH84001. Science 273, 924–930 (5277).

McNeil, J.R., Reid, R.D., Gerstenberger, D.C., Collins, G.J., 1978. Ultra-Violet Ion Lasers. Opt. Laser Technol. 10 (3), 138–140. doi:10.1016/0030-3992(78)90060-9.

Merkulov, V.I., Lannin, J.S., Munro, C.H., Asher, S.A., Veerasamy, V.S., Milne, W.I., 1997. UV Studies of tetrahedral bonding in diamond-like amorphous carbon. Phys. Rev. Lett. 78 (25), 4869–4872.

Ming, D.W., Archer Jr., P.D., Glavin, D.P., Eigenbrode, J.L., Franz, H.B., et al., 2014. Volatile and Organic Compositions of Sedimentary Rocks in Yellowknife Bay, Gale Crater, Mars. Science 343 (6169). doi:10.1126/science.1245267.

Misra, A.K., Sharma, S.K., Bates, D.E., Acosta, T.E., 2010. Compact standoff Raman system for detection of homemade explosives. SPIE Defense, Security, and Sensing 76650U-76650 U doi:10.1117/12.849850.

Navarro-González, R., Vargas, E., de la Rosa, José, Raga, A.C., McKay, C.P., 2010. Reanalysis of the Viking results suggests perchlorate and organics at midlatitudes on Mars. J. Geophys. Res. 115 (E12010). doi:10.1029/2010JE003599.

Navarro-González, R., Stern, J., Sutter, B., Archer, D., McAdam, A., et al. 2013. Possible Detection of Nitrates on Mars by the Sample Analysis at Mars (SAM) Instrument. Abstract #2648 presented at the 44th Lunar and Planetary Science Conference.

Nelson, W.H., Manoharan, R., Sperry, J.F., 1992. UV Resonance Raman Studies of Bacteria. Appl. Spectroscopy Rev. 27 (1), 67–124.

Nelson, W.H., Sperry, J.F., 1991. UV resonance Raman spectroscopic detection and identification of bacteria and other microorganisms. In: Nelson, W.H. (Ed.), Modern Techniques for Rapid Microbiological Analysis. VCH Publisher, New York, pp. 97–143. (1991).

Niles, P.B., Catling, D.C., Berger, G., Chassefiere, E., Ehlmann, B.L., Michalski, J.R., Morris, R., Ruff, S.W., Sutter, B., 2013. Geochemistry of carbonates on Mars: implications for climate history and nature of aqueous environments. Space Sci. Rev. 174 (1-4), 301–328.

Osterrothova, K., Jehlicka, J., 2010. Raman spectroscopic identification of phthalic and mellitic acids in mineral matrices. Spectrochimica Acta Part A 77 (5), 1092–1098.

Peters, G.H., Abbey, W., Bearman, G.H., Mungas, G.S., Smith, J.A., Anderson, R.C., Douglas, S., Beegle, L.W., 2008. Mojave Mars Simulant - Characterization of a new geologic Mars analog. Icarus 197, 470–479.

Pierazzo, E., Chyba, C.F., 1999. Amino Acid survival in large cometary impacts. Meteorit. Planet. Sci. 34, 909–918.

Popp, J., Tarcae, N., Kiefer, W., Hilchenbach, M., Thomas, N., Hofer, S., Stuffler, T., 2001. Investigations on Mars Model Minerals by in situ Laser Raman Spectroscopy. ESA Supplemental Publication 496, 193–196.

Rava, R.P., Spiro, T.G., 1985. Resonance enhancement in the ultraviolet Raman spectra of aromatic amino acids. J. Phys. Chem. 89 (10), 1856–1861.

Rietveld, H.M., 1969. A profile refinement method for nuclear and magnetic structures. J.Appl. Crystallogr. 2, 65–71.

Rividi, N., van Zuilen, M., Philippot, P., Menez, B., Godard, G., Poidatz, E., 2010. Calibration of Carbonate Composition Using Micro-Raman Analysis: Application to Planetary Surface Exploration. Astrobiology 10 (3), 293–309 doi:10.1089=ast.2009.0388.

Rousseau, D.L., Miller, R.E., Leroi, G.E., 1968. Raman Spectrum of Crystalline Sodium Nitrate. J. Chem. Phys. 48 (8), 3409–3413.

Rull, F., Sansano, A., Diaz, E., Canora, C.P., Moral, A.G., et al., 2011. ExoMars Raman laser spectrometer for Exomars. In: Proceedings SPIE 8152, p. 12.

Skulinova, M., Lefebvre, C., Sobron, P., Eshelman, E., Daly, M., Gravel, J.F., Cormier, J.F., Chateauneuf, F., Slater, G., Zheng, W., Koujelev, A., Leveille, R., 2014. Time-resolved stand-off UV-Raman spectroscopy for planetary exploration. Planet. Space Sci. 92, 88–100. doi:10.1016/j.pss.2014.01.010.

Smith, E., Dent, G., 2005. Modern Raman Spectroscopy: A Practical Approach. John Wiley & Sons, Chichester.

Socrates, G., 2001. Infrared and Raman Characteristic Group Frequencies: Tables and Charts. John Wiley & Sons, Chichester.

Stalport, F., Coll, P., Szopa, C., Cottin, H., Raulin, F., 2009. Investigating the Photostability of Carboxylic Acids Exposed to Mars Surface Ultraviolet Radiation Conditions. Astrobiology 9 (6), 543–549. doi:10.1089/ast.2008.0300.

Steele, A., McCubbin, F.M., Fries, M., Kater, L., Boctor, N.Z., et al., 2012a. A Reduced Organic Carbon Component in Martian Basalts. Science 337, 212–215 (6091).

Steele, A., McCubbin, F.M., Fries, M.D., Golden, D.C., Ming, D.W., Benning, L.G., 2012b. Graphite in the martian meteorite Allan Hills 84001. Am. Mineralogist 97 (7), 1256–1259. doi:10.2138/am.2012.4148.

Stern, J.C., Sutter, B., Freissinet, C., Navarro-Gonzalez, R., McKay, C.P., et al., 2015. Evidence for indigenous nitrogen in sedimentary and aeolian deposits from the *Curiosity* rover investigations at Gale crater, Mars. In: Proceedings of the National Academy of Sciences Early Edition doi:10.1073/pnas.1420932112.

Stoker, C.R., Bullock, M.A., 1997. Organic degradation under simulated Martian conditions. J. Geophys. Res. 102 (E5) 10,881-10,888.

Storrie-Lombardi, M.C., Hug, W.F., McDonald, G.D., Tsapin, A.I., Nelson, K.H., 2001. Hollow Cathode Ion Lasers for Deep Ultraviolet Raman Spectroscopy and Fluorescence Imaging. Rev. Sci. Instrum. 72 (12), 4452–4459.

Swayze, G.A., Ehlmann, B.L., Milliken, R.E., Poulet, F., Gray, J.J., et al., Discovery of the Acid-Sulfate Mineral Alunite in Terra Sirenum, Mars, Using MRO CRISM: Possible Evidence for Acid-Saline Lacustrine Deposits? Abstract #P44A-04 presented at the American Geophysical Union, Fall Meeting 2008.

Tarcea, N., Harz, M., Rosch, P., Frosch, T., Schmitt, M., Thiele, H., Hochleitner, R., Popp, Jurgen., 2007. UV Raman spectroscopy - A technique for biological and mineralogical in situ planetary studies. Spectrochimica Acta Part A 68, 1029–1035.

ten Kate, I.L., 2010. Organics on Mars? Astrobiology 10 (6), 589–603.

ten Kate, I.L., Garry, J.R.C., Peeters, Z., Foing, B., Ehrenfreund, P., 2006. The effects of Martian near surface conditions on the photochemistry of amino acids. Planet. Space Sci. 54, 296–302.

Vaniman, D.T., Bish, D.L., Ming, D.W., Bristol, T.F., Morris, R.V., et al., 2013. Mineralogy of a Mudstone at Yellowknife Bay, Gale Crater, Mars. Science 342. doi:10.1126/ science.1243480.

Vitek, P., Osterrothova, K., Jehlicka, J., 2009. Beta-carotene - A possible biomarker in the Martian evaporitic environment: Raman micro-spectroscopic study. Planet. Space Sci. 57, 454–459.

Wang, A., Freeman, J.J., Jolliff, B.L., Chou, I.M., 2006. Sulfates on Mars: A systematic Raman spectroscopic study of hydration states of magnesium sulfates. Geochimica et Cosmochimica Acta 70, 6118–6135.

Wang, A., Haskin, L.A., Lane, A.L., Wdowiak, T.J., Squyres, S.W., Wilson, R.J., Hovland, L.E., Manatt, K.S., Raouf, N., Smith, C.D., 2003. Development of the Mars Microbeam Raman Spectrometer (MMRS). J. Geophys. Res. 108 (E1), 5005. doi:10.1029/2002JE00190.

Wise, W.S., Kleck, W.D., 1988. Sodic Clay-Zeolite Assemblage in Basalt at Boron, California. Clays Clay Miner. 36 (2), 131–136.

Wray, J.J., Milliken, R.E., Dundas, C.M., Swayze, G.A., Andrews-Hanna, J.C., et al., 2011. Columbus crater and other possible groundwater-fed paleolakes of Terra Sirenum, Mars. J. Geophys. Res., Planets 116 (E1). doi:10.1029/2010JE003694.

Wu, Q., Hamilton, T., Nelson, W.H., Elliott, S., Sperry, J.F., Wu, M., 2001. UV Raman Spectral Intensities of E. Coli and Other Bacteria Excited at 228.9, 244.0, and 248.2 nm. Anal. Chem. 73 (14), 3432–3440.

Wu, Z., Zhang, C., Stair, P.C., 2006. Influence of absorption on quantitative analysis in Raman spectroscopy. Catal. Today 113, 40–47.

Zhu, G., Zhu, X., Fan, Q., Wan, X., 2011. Raman spectra of amino acids and their aqueous solutions. Spectrochimica Acta Part A 78, 1187–1195.